Limits on Anisotropy in the Nanohertz Stochastic Gravitational Wave Background

S. R. Taylor,[1,2,*] C. M. F. Mingarelli,[3,4,5] J. R. Gair,[2] A. Sesana,[5,6] G. Theureau,[7,8,9] S. Babak,[6] C. G. Bassa,[10,11] P. Brem,[6] M. Burgay,[12] R. N. Caballero,[4] D. J. Champion,[4] I. Cognard,[7,8] G. Desvignes,[4] L. Guillemot,[7,8] J. W. T. Hessels,[10,13] G. H. Janssen,[10,11] R. Karuppusamy,[4] M. Kramer,[4,11] A. Lassus,[4,7] P. Lazarus,[4] L. Lentati,[14] K. Liu,[4] S. Osłowski,[15,4] D. Perrodin,[12] A. Petiteau,[16] A. Possenti,[12] M. B. Purver,[11] P. A. Rosado,[17,18] S. A. Sanidas,[11,13] R. Smits,[10] B. Stappers,[11] C. Tiburzi,[12,19] R. van Haasteren,[1] A. Vecchio,[5] and J. P. W. Verbiest[15,4]

(EPTA Collaboration)

[1]*Jet Propulsion Laboratory, California Institute of Technology, Pasadena, California 91109, USA*
[2]*Institute of Astronomy, University of Cambridge, Madingley Road, Cambridge CB3 0HA, United Kingdom*
[3]*TAPIR (Theoretical Astrophysics), California Institute of Technology, MC 350-17, Pasadena, California 91125, USA*
[4]*Max-Planck-Institut für Radioastronomie, Auf dem Hügel 69, D-53121 Bonn, Germany*
[5]*School of Physics and Astronomy, University of Birmingham, Edgbaston, Birmingham B15 2TT, United Kingdom*
[6]*Max-Planck-Institut für Gravitationsphysik, Albert Einstein Institut, Am Mühlenberg 1, 14476 Golm, Germany*
[7]*Laboratoire de Physique et Chimie de l'Environnement et de l'Espace LPC2E CNRS-Université d'Orléans, F-45071 Orléans, France*
[8]*Station de radioastronomie de Nançay, Observatoire de Paris, CNRS/INSU, F-18330 Nançay, France*
[9]*Laboratoire Univers et Théories LUTh, Observatoire de Paris, CNRS/INSU, Université Paris Diderot, 5 place Jules Janssen, 92190 Meudon, France*
[10]*ASTRON, the Netherlands Institute for Radio Astronomy, Postbus 2, 7990 AA Dwingeloo, Netherlands*
[11]*Jodrell Bank Centre for Astrophysics, University of Manchester, Manchester M13 9PL, United Kingdom*
[12]*INAF—Osservatorio Astronomico di Cagliari, via della Scienza 5, I-09047 Selargius, CA, Italy*
[13]*Anton Pannekoek Institute for Astronomy, University of Amsterdam, Science Park 904, 1098 XH Amsterdam, Netherlands*
[14]*Astrophysics Group, Cavendish Laboratory, JJ Thomson Avenue, Cambridge CB3 0HE, United Kingdom*
[15]*Fakultät für Physik, Universität Bielefeld, Postfach 100131, 33501 Bielefeld, Germany*
[16]*Université Paris-Diderot-Paris7, APC—UFR de Physique, Batiment Condorcet, 10 rue Alice Domont et Léonie Duquet, 75205 Paris Cedex 13, France*
[17]*Centre for Astrophysics and Supercomputing, Swinburne University of Technology, P.O. Box 218, Hawthorn VIC 3122, Australia*
[18]*Max Planck Institute for Gravitational Physics, Albert Einstein Institute, Callinstraße 38, 30167 Hanover, Germany*
[19]*Dipartimento di Fisica—Universitá di Cagliari, Cittadella Universitaria, I-09042 Monserrato, CA, Italy*

(Received 21 May 2015; published 22 July 2015)

The paucity of observed supermassive black hole binaries (SMBHBs) may imply that the gravitational wave background (GWB) from this population is anisotropic, rendering existing analyses suboptimal. We present the first constraints on the angular distribution of a nanohertz stochastic GWB from circular, inspiral-driven SMBHBs using the 2015 European Pulsar Timing Array data. Our analysis of the GWB in the ∼2–90 nHz band shows consistency with isotropy, with the strain amplitude in $l > 0$ spherical harmonic multipoles $\lesssim$40% of the monopole value. We expect that these more general techniques will become standard tools to probe the angular distribution of source populations.

DOI: 10.1103/PhysRevLett.115.041101 PACS numbers: 04.80.Nn, 04.30.-w, 97.60.Gb, 98.65.Fz

Introduction.—Pulsar timing arrays (PTAs) are currently being used to search for, and to eventually characterize, the nanohertz stochastic gravitational wave background (SGWB) by looking for correlated deviations in the pulse times of arrival (TOAs) of multiple radio millisecond pulsars distributed across the sky. The SGWB in the nanohertz regime is thought to be generated by the incoherent superposition of a large number of weak and unresolved GW sources, including supermassive black hole binaries (SMBHBs) [1–7], decaying cosmic-string networks [8–11], or primordial GWs [12,13]. Previous analyses have assumed background isotropy, which emerges as a special case from the more general anisotropy framework presented here. Although GWs have not yet been directly detected, limits on the angular power distribution of a nanohertz SGWB may constrain the distribution of low redshift structure [14], the location of several particularly bright nearby sources dominating the signal strain budget [15,16], and open a new avenue to explore the population characteristics of SMBHBs. Moreover, if a significant fraction of SMBHBs stall rather than merge, or are rapidly driven to merger via strong couplings to the

galactic nuclear environment, then we may expect a depleted nanohertz GW signal dominated by only a few bright sources [17]. As such, the tools implemented here may provide new and novel insights into the final-parsec problem (see, e.g., Ref. [18]). This research is a result of the common effort to directly detect gravitational waves using pulsar timing, known as the European Pulsar Timing Array (EPTA) [19,20].

Limits on the SGWB are usually reported in terms of the characteristic-strain spectrum $h_c(f)$ of a background that is composed of purely GW-driven, circular, inspiraling SMBHBs, which obeys a simple power law

$$h_c(f) = A_h(f/\mathrm{yr}^{-1})^{-2/3}, \quad (1)$$

where A_h is the strain amplitude reported at a reference frequency $f = \mathrm{yr}^{-1}$ [21]. The correlations induced by a SGWB in pulsar TOAs can be understood by considering a perturbation to the space-time metric along the Earth-pulsar line of sight causing a change in the perceived rotational frequency of the pulsar [22–25]. The fractional frequency shift $\delta\nu(t)/\nu_0$ of a signal from a pulsar at rest frequency ν_0 is the difference in the metric perturbation at the Solar System barycenter (SSB), and at the pulsar. This frequency shift is integrated over time to give the induced timing residuals, $r(t) \equiv \int^t \delta\nu(t')/\nu_0 dt'$, which are cross-correlated between pulsars in an effort to boost the detection probability of GW signals at Earth. The expectation value of the cross-correlated timing residuals between pulsars a and b is proportional to the overlap reduction function (ORF, Γ_{ab})—a dimensionless function that quantifies the response of a pair of pulsars to the stochastic GW background [26,27]. In this Letter, we use analytically computed anisotropic ORFs [28,29] and recently developed Bayesian techniques [30] to constrain the angular power distribution of the SGWB.

Fitting a pulsar timing model.—The average pulse profiles of millisecond pulsars are remarkably stable and reproducible. This stability permits high-precision timing, which is crucial to GW searches: the minimum detectable GW strain is $h_c \propto 10^{-15}(\sigma_{\mathrm{rms}}/100\ \mathrm{ns})(T/10\ \mathrm{yr})^{-1}$, where σ_{rms} is the root-mean-square of the pulsar timing residuals, and T is the total observation time span [5]. Therefore, high timing precision and long-term observations are required to distinguish the GW signal from noise, as well as boost the signal-to-noise ratio (SNR) in a search.

Pulsar observations lead to a catalog of TOAs, which can then be analyzed to search for GWs. A timing model describing all deterministic contributions to a pulsar's TOAs [rotational frequency, spin-down rate, dispersion measure (DM), etc.] is iteratively fit with the analysis package, TEMPO2 [31,32]. The difference between the measured TOAs and the refined timing model prediction is the post-fit timing residual, which constitutes the input data in our GW analysis.

GW analysis pipeline.—We use the signal modeling techniques described in Ref. [33] (from hereon L15). The posterior probability of the model parameters $\vec{\Theta}$, given the concatenated post-fit timing residuals from all pulsars $\vec{\delta t}$, is a multivariate Gaussian:

$$p(\vec{\Theta}|\vec{\delta t}) \propto p(\vec{\Theta}) \frac{\exp\left(-\frac{1}{2}\vec{\delta t}^{\mathrm{T}}\mathbf{G}(\mathbf{G}^{\mathrm{T}}\mathbf{C}\mathbf{G})^{-1}\mathbf{G}^{\mathrm{T}}\vec{\delta t}\right)}{\sqrt{\det\left[2\pi(\mathbf{G}^{\mathrm{T}}\mathbf{C}\mathbf{G})\right]}}, \quad (2)$$

where $p(\vec{\Theta})$ is the prior probability distribution of model parameters, and projecting all quantities with the matrix $\mathbf{G}$ marginalizes this posterior probability over all timing model parameters (see Ref. [34]). The covariance of the *pre-fit* timing residuals is defined as $\mathbf{C} = \mathbf{C}_{\mathrm{red}} + \mathbf{N}$, where $\mathbf{C}_{\mathrm{red}}$ includes the SGWB, intrinsic pulsar red noise, and DM variation components, while $\mathbf{N}$ denotes all white-noise components. This red covariance is decomposed in terms of a low-rank approximation such that $\mathbf{C}_{\mathrm{red}} = \mathbf{F}\boldsymbol{\varphi}\mathbf{F}^T$, where $\mathbf{F}$ is a block-diagonal matrix of Fourier basis vectors, and $\boldsymbol{\varphi}$ is a spectral covariance matrix [35–37]. Intrinsic red noise and SGWB are expanded in the same Fourier basis, while the DM-variation signal is expanded in basis functions that differ only by an extra multiplicative factor of $\propto 1/\nu_o^2$, where ν_o is the observing frequency of the pulses. The matrix $\mathbf{N}$ is diagonal, with entries given by the squared TOA errors that have been corrected by previous single pulsar analyses [33]. We apply a multiplicative factor to all error bars of a given pulsar (referred to as the GEFAC parameter) which is searched over here.

The matrix $\boldsymbol{\varphi}$ has band-diagonal structure, since Fourier modes between different pulsars may be correlated due to the presence of a SGWB or correlated noise. Therefore,

$$[\boldsymbol{\varphi}]_{ai,bj} = \Gamma_{ab}\rho_i\delta_{ij} + \epsilon_i\delta_{ij} + \eta_i\delta_{ab}\delta_{ij} + \kappa_{ai}\delta_{ab}\delta_{ij}, \quad (3)$$

where i and j index the discretely sampled signal or noise frequencies in our analysis of pulsar TOAs; $\rho = h_c(f)^2/(12\pi^2 f^3 T_{\mathrm{max}})$ is the power spectrum of the SGWB, with T_{max} equal to the timing baseline of the PTA; ϵ is the spectrum of a completely correlated red-noise process, which may result from modeling inaccuracies due to drifts in the observatory and global time standards; η is the spectrum of a common, but uncorrelated, red-noise process that may originate from common physical processes inside the neutron stars, see, e.g., Refs. [38,39]; and κ_a is the individual red-noise and DM-variation spectrum for pulsar a. All these spectra are modeled with power laws, $(A^2/12\pi^2 T_{\mathrm{max}})(f_n/\mathrm{yr}^{-1})^{2\alpha-3}\ \mathrm{yr}^2$, where $A = A_h$ for the SGWB; α is a spectral index that equals $-2/3$ for the SGWB; and f_n are the n frequencies at which we sample the spectra of red-noise processes, where in this analysis $n = 50$.

The ORF Γ_{ab} is the average of the overlap of the pulsars' antenna response functions $F_a^A(\hat{\Omega})$ (see, e.g., Refs. [28,30]),

over GW propagation directions $\hat{\Omega}$, and weighted by the SGWB angular power distribution $P(\hat{\Omega})$:

$$\Gamma_{ab} = \frac{3}{8\pi}(1+\delta_{ab})\int_{S^2} d\hat{\Omega} P(\hat{\Omega}) \sum_q F_a^q(\hat{\Omega}) F_b^q(\hat{\Omega}), \quad (4)$$

where q labels the $\{+,\times\}$ GW polarization. An excess in $P(\hat{\Omega})$ in a particular region of the sky may indicate a particularly bright single source, or a hot spot of several sources [28,30,40,41]. In the following, we decompose the SGWB angular distribution such that $P(\hat{\Omega}) \equiv \sum_{l=0}^{l_{\max}} \sum_{m=-l}^{l} c_{lm} Y_{lm}(\hat{\Omega})$, with normalization $\int_{S^2} P(\hat{\Omega}) d\hat{\Omega} = 4\pi$, where Y_{lm} are the real spherical harmonics. Inserting this decomposition into Eq. (4) and proceeding as in Ref. [28], we expand Γ_{ab} into a sum over anisotropic ORFs, $\Gamma_{lm}^{(ab)}$, with associated weights c_{lm} to be constrained by the analysis and which characterize the SGWB angular power distribution. We note that the leading function in this expansion, $c_{00}\Gamma_{00}^{(ab)}$, corresponds to the ORF applicable to the monopole moment of $P(\hat{\Omega})$ (also known as the Hellings and Downs curve [42]). Hence, current analysis strategies for isotropic SGWBs emerge from our fully general anisotropy framework as a special case.

Each pulsar has 5 stochastic parameters to be constrained in a Bayesian analysis: intrinsic red noise (A,α), DM variation (A,α), and a GEFAC parameter. The fully correlated red-noise component ϵ will contribute 2 power-law parameters, as will the common, uncorrelated process η. The spectrum of the SGWB is modeled with a fixed slope of $-2/3$ and an amplitude A_h to be constrained, while $l_{\max} > 0$ analyses will include $[(l_{\max}+1)^2 - 1]$ additional parameters. The priors on the parameters are $\log_{10} A \in U[-20,-10]$, $\alpha \in U[-2.0, 1.5]$, GEFAC $\in U[0.1, 10.0]$. The c_{lm} coefficients are constrained by a prior requiring the implied distribution of GW power to be positive at all sky locations [30], called the "physical prior". The prior on A_h is treated separately from other red-noise components, and is uniform in the range $[10^{-20}, 10^{-10}]$. Applying a uniform prior on A_h with logarithmic priors on the amplitudes of all other red components will provide the most conservative upper limits on the strain-spectrum amplitude of the SGWB.

Results.—We parametrize the angular distribution of the SGWB down to the angular resolution of the PTA. The most anisotropic SGWB signal is one dominated by a single source. Hence the angular resolution, and thus $l_{\max}$, is a function of the number of pulsars, $N_{\rm psr}$, which significantly contribute to a single-source detection, and the SNR of that detection [43]. Sesana and Vecchio [43] find that the angular resolution of a PTA for a resolvable GW source is $\Delta\Omega \propto 50(50/N_{\rm psr})^{1/2}(10/{\rm SNR})^2$ deg^2, and this resolution sets an upper bound on l via $l = 180/\theta$, where $\theta = \sqrt{\Delta\Omega}$ [29]. We analyze a subset of the six best pulsars in the EPTA [19] that encapsulate ~95% of the full-array SNR in simulated continuous GW searches [44]: PSRs J0613−0200, J1012+5307, J1600−3053, J1713+0747, J1744−1134, J1909−3744, where $T_{\max} = 17.7$ years and the GW frequencies with which we characterize red-noise components are $\in [1/T_{\max} = 1.79, 50/T_{\max} = 89.7$ nHz$]$. Hence, in our array subset $l_{\max} \lesssim 4$. Carrying out searches with the noise characteristics of each pulsar fixed, we find the upper limits on the strain amplitude remain consistent whether we analyze this six-pulsar subset or the full array. Including more pulsars of comparably high timing quality would contribute a larger number of pulsar pairs $[N_{\rm pairs} = N_{\rm psr}(N_{\rm psr}-1)/2]$, which would serve to increase the SNR and resolving power ($l_{\max}$) of any search for anisotropy. This comes at the cost of longer likelihood evaluation times, making the systematic study presented here currently intractable. Our goal is to provide the first constraints on anisotropy in the SGWB via a systematic study with current techniques—we do so with the 15 distinct pulsar pairings afforded by a six-pulsar array. All analysis is performed with parallel-tempering Markov chain Monte Carlo (MCMC) analysis.

The 95% upper limits on A_h from our analyses are shown in Table I. First, we perform searches with a single set of anisotropy coefficients c_{lm} across the entire band, which we call the all-band anisotropy parametrization, (cf. Table I). We also perform frequency-dependent searches by parametrizing each frequency with independent $c_{lm}(f)$ coefficients. We split our band into 5 equal subbands ($\Delta f = 17.9$ nHz), and independent $c_{lm}(f)$ coefficients constrained in each, called the frequency-dependent anisotropy parametrization (i). Finally, motivated by the results of L15—where most of the SGWB constraints were found to come from the lowest three frequencies—we apply independent $c_{lm}(f)$ coefficients to the lowest four frequencies in our analysis $(f = [1,2,3,4]/T_{\max} = [1.79, 3.59, 5.38, 7.18]$ nHz), with the remainder of the band $(f = [5,\ldots,50]/T_{\max} = [8.98,\ldots,89.7]$nHz) parametrized by a single set of coefficients. This is reported as frequency-dependent

TABLE I. 95% upper limits on SGWB strain amplitude A_h. The first column is the all-band anisotropy parametrization, the second and third correspond to the frequency-dependent anisotropy parametrizations (i) and (ii), respectively, described in the text.

$l_{\max}$	A_h; all-band c_{lm}	A_h; $c_{lm} = c_{lm}(f)^{(i)}$	A_h; $c_{lm} = c_{lm}(f)^{(ii)}$
0	3.94×10^{-15}	N/A	N/A
1	4.09×10^{-15}	4.06×10^{-15}	4.06×10^{-15}
2	4.06×10^{-15}	4.07×10^{-15}	4.02×10^{-15}
3	4.06×10^{-15}	3.98×10^{-15}	4.01×10^{-15}
4	4.03×10^{-15}	3.95×10^{-15}	3.99×10^{-15}

anisotropy parametrization (ii). The recovered upper limit does not deteriorate through the increased number of parameters in our higher multipole searches. The monopole upper limits do not precisely match those found in L15 due to several variations in the analysis specifics: namely, (i) our prior on the amplitude of red-noise components is uniform in logarithm of the amplitudes, which provides a more conservative upper limit on the SGWB strain amplitude; (ii) we do not consider Solar System ephemeris errors in our correlated noise modeling; and (iii) we employed a pure time-domain likelihood in the initial single pulsar analysis to correct the TOA errors in each pulsar. Hence, our monopole upper limits are higher than in L15 by $\sim 1 \times 10^{-15}$. However, moving beyond the first analysis presented here, our more general anisotropy framework can be easily incorporated into all existing and planned pipelines to become a standard tool set, since it recovers the isotropic SGWB constraints as a special case. The upper limits on the strain amplitude in each anisotropic multipole of the search are shown in the left panel of Fig. 1, where the constraints are entirely dominated by the restrictions imposed on the c_{lm}'s by the physical prior. Our data are not informative enough to update the prior knowledge we have about the anisotropy of the GW sky.

Rather than impose a specific decomposition of the SGWB sky during sampling, we can recover the cross-correlation values between pulsar pairs and map these to a chosen basis in postprocessing. We perform a Bayesian search for the distinct elements of the Cholesky factor of the residual cross-correlation matrix, which ensures positive definiteness of the final matrix [35,45]. After sampling we define a mapping between the coefficients of the ORF in a particular basis, $\vec{c}$, and the cross-correlation values, $\vec{\Gamma}$, such that $\vec{\Gamma} = \mathbf{H}\vec{c}$. A single row of the matrix $\mathbf{H}$ will have entries corresponding to the ORF between pulsars a and b evaluated for all basis terms. In the spherical-harmonic basis, such a row would consist of $(\Gamma_{00}^{(ab)}\Gamma_{1-1}^{(ab)}\cdots\Gamma_{lm}^{(ab)})$, and for a pixel basis this is $(\Gamma_{\hat{\Omega}_1}^{(ab)}\Gamma_{\hat{\Omega}_2}^{(ab)}\cdots\Gamma_{\hat{\Omega}_N}^{(ab)})$. Having recovered posterior samples of the vector $\vec{\Gamma}$, we map these to samples of $\vec{c}$ via $\vec{c} = \mathbf{H}^{+}\vec{\Gamma}$, where $\mathbf{H}^{+}$ corresponds to the Moore-Penrose pseudoinverse of the matrix $\mathbf{H}$ [46,47]. The results for mappings to the spherical-harmonic basis with varying $l_{\max}$ are shown in Fig. 1 (right). The data support such strong anisotropy signatures in this model because the joint posterior in the cross-correlation values are consistent with essentially the entire range of $[-1, 1]$, which when mapped to a spherical-harmonic ORF basis leads to large c_{lm} values. There is nothing to penalize these large anisotropy coefficients, which lead to highly anisotropic (and possibly negative) GW power distributions and would otherwise be restricted by the physical prior. This supports our claim that the constraints in Fig. 1 (left) are prior dominated.

We also map our recovered cross-correlation samples to a pixel basis with 12288 equal-area pixels on the sky. We supplement our mapping with the additional normalization constraint that $\int_{S^2} P(\hat{\Omega})d\hat{\Omega} \approx \sum_{i=1}^{N_{\rm pix}} c(\hat{\Omega}_i)\Delta\hat{\Omega}_i = 4\pi$. The resulting SGWB power in each pixel is marginalized over all other pixels and truncated to obtain the positive 1D-marginalized power PDF before it is integrated over to obtain the upper limit on the strain amplitude in that pixel. The result is shown in Fig. 2, where we see the distinctive overlapping antenna patterns of the pulsars mapping out the sensitivity of the PTA to the background strain amplitude. The constraints on A_h from each pixel are quite poor, and in some cases are more than an order of magnitude worse than the all-sky upper limit. As we decrease the resolution of the

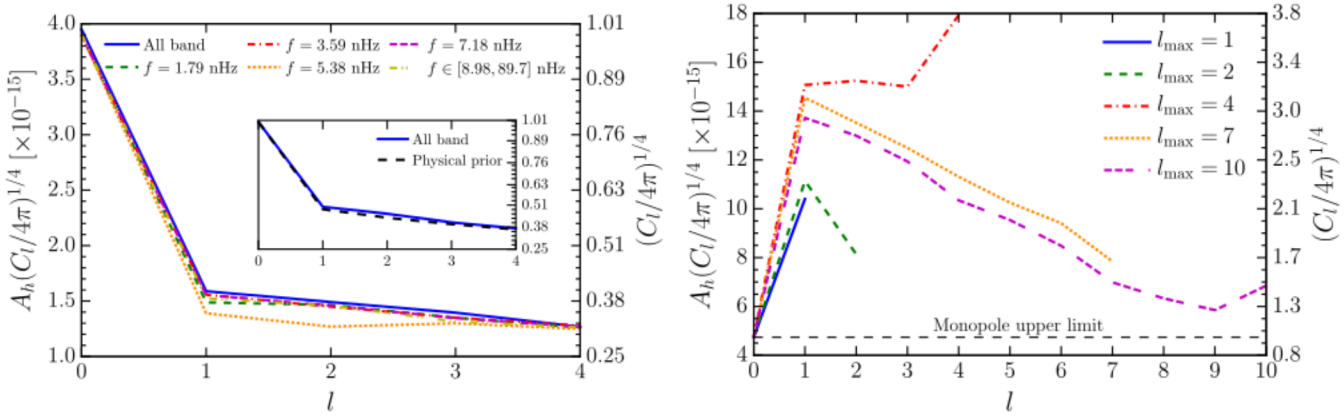

FIG. 1 (color online). 95% upper limits on the strain amplitude, where $C_l = \sum_{m=-l}^{l} |c_{lm}|^2/(2l+1)$. Left: all-band anisotropy parametrization and frequency-dependent parametrization (ii). The right axis is the ratio of the upper limit to the monopole. The inset figure shows 95% upper limits on $(C_l/4\pi)^{1/4}$, which are marginalized over the strain amplitude for the all-band anisotropy parametrization and a constant likelihood analysis. Our limits reflect the constraints of the physical prior. Right: all-band anisotropy parametrization, where the c_{lm} values are obtained by mapping cross-correlation values to the spherical harmonic basis, without physical prior rejection.

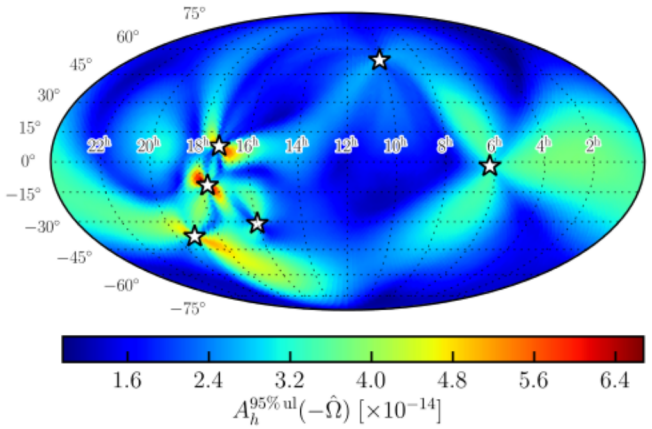

FIG. 2 (color online). 95% upper limits on the GW strain amplitude in each pixel. These limits are obtained by mapping from the Bayesian MCMC-sampled cross-correlation values to a pixelated ORF basis ($N_{\mathrm{pix}} = 12\,288$). White stars show the pulsar locations.

pixelation the constraints in each pixel become tighter, until we reach the limit of one pixel, which recovers the usual all-sky upper limit. Figure 2 can also help to explain the results in the right panel of Fig. 1, where we see that the distribution of pulsars in our array leads to the suboptimal overlapping of the antenna response functions, which in turn causes insensitivities around the 4 clustered pulsars and on large angular scales. Hence, we will lack sensitivity to large angular scale anisotropy ($l \sim 1$), which is reflected in the right panel of Fig. 1. Moreover, this sensitivity map illustrates the importance of timing pulsars from all over the sky to ensure a more uniform sensitivity to GW strain, which will be possible through international collaborations such as the International PTA [48].

Conclusions.—Our analyses suggest that this data set is not informative enough to update our prior knowledge of the angular distribution of the nanohertz SGWB. Using a prior that enforces a positive SGWB distribution, we find that the 95% upper limit on the strain amplitude in multipoles of the background distribution with $l > 0$ is $\lesssim$40% of the monopole strain. No evolution of these upper limits as a function of GW frequency is found since the constraints are a reflection of the prior. Additionally, we can recover the joint posterior distribution of the cross-correlation values between pulsar pairings, and subsequently map these to a spherical-harmonic or pixel ORF basis. With the only constraint being positive definiteness of the cross-correlation matrix, the strain amplitude in $l > 0$ multipoles is $\lesssim$400% of the monopole value. The strain-amplitude upper limits as a function of location on the sky reflect the overlapping antenna pattern behavior of the full PTA, where the limits can often be more than an order of magnitude worse than the all-sky limit. A full description of all techniques employed here, and their efficacy, will be provided in a follow-up methods paper.

Forthcoming advanced radio instruments such as the Five-Hundred-Metre Aperture Spherical Radio Telescope [49,50], MeerKAT [51], and the Square Kilometre Array [52] will enhance the detection and inference prospects for anisotropic GW skies by detecting large numbers of millisecond pulsars and timing them to unprecedented precision. Upcoming studies will investigate how we can combine galaxy catalogs with frequency-dependent maps of the nanohertz GW sky to probe whether the strain budget is being dominated by a few bright nearby sources, or is more diffuse. We hope that the work presented here, together with these future studies, will provide important insights into the demographics, evolution, and assembly of SMBHBs not accessible by any other means.

This work was carried out under the aegis of the EPTA. Part of this work is based on observations with the 100-m telescope of the Max-Planck-Institut für Radioastronomie (MPIfR) at Effelsberg. The Nançay Radio Observatory is operated by the Paris Observatory, associated to the French Centre National de la Recherche Scientifique (CNRS). We acknowledge financial support from "Programme National de Cosmologie and Galaxies" (PNCG) of CNRS/INSU, France. Pulsar research at the Jodrell Bank Centre for Astrophysics and the observations using the Lovell telescope is supported by a consolidated grant from the STFC in the UK. The Westerbork Synthesis Radio Telescope is operated by the Netherlands Institute for Radio Astronomy (ASTRON) with support from The Netherlands Foundation for Scientific Research NWO. S. R. T. acknowledges the support of the STFC and the RAS. This research was in part supported by S. R. T's appointment to the NASA Postdoctoral Program at the Jet Propulsion Laboratory, administered by Oak Ridge Associated Universities through a contract with NASA. C. M. F. M. was supported by a Marie Curie International Outgoing Fellowship within the 7th European Community Framework Programme. This research was performed in part using the Zwicky computer cluster at Caltech supported by NSF under MRI-R2 award No. PHY-0960291 and by the Sherman Fairchild Foundation. This work was in part performed using the Darwin Supercomputer of the University of Cambridge High Performance Computing Service, provided by Dell Inc. using Strategic Research Infrastructure Funding from the Higher Education Funding Council for England and funding from the STFC. A. S. and J. G. are supported by the Royal Society. L. L. was supported by a Junior Research Fellowship at Trinity Hall College, Cambridge University. S. A. S. acknowledges funding from an NWO Vidi fellowship (PI: J. W. T. H.). R. N. C. acknowledges the support of the International Max Planck Research School Bonn/Cologne and the Bonn-Cologne Graduate School. K. J. L. is supported by the National Natural Science Foundation of China (Grant No. 11373011). R. vH. is supported by NASA Einstein Fellowship grant PF3-140116. J. W. T. H. acknowledges funding from an

NWO Vidi fellowship and ERC Starting Grant 'DRAGNET' (337062). P. L. acknowledges the support of the International Max Planck Research School Bonn/Cologne. K. L. acknowledges the financial support by the European Research Council for the ERC Synergy Grant BlackHoleCam under Contract No. 610058. S. O. is supported by the Alexander von Humboldt Foundation. The authors also acknowledge support of NSF Award No. PHY-1066293 and the hospitality of the Aspen Center for Physics.

*Stephen.R.Taylor@jpl.nasa.gov

[1] M. Rajagopal and R. W. Romani, Astrophys. J. **446**, 543 (1995).
[2] J. S. B. Wyithe and A. Loeb, Astrophys. J. **590**, 691 (2003).
[3] A. H. Jaffe and D. C. Backer, Astrophys. J. **583**, 616 (2003).
[4] A. Sesana, A. Vecchio, and M. Volonteri, Mon. Not. R. Astron. Soc. **394**, 2255 (2009).
[5] A. Sesana, A. Vecchio, and C. N. Colacino, Mon. Not. R. Astron. Soc. **390**, 192 (2008).
[6] Z. L. Wen, F. A. Jenet, D. Yardley, G. B. Hobbs, and R. N. Manchester, Astrophys. J. **730**, 29 (2011).
[7] A. Sesana, Classical Quantum Gravity **30**, 244009 (2013).
[8] A. Vilenkin, Phys. Rev. D **24**, 2082 (1981).
[9] A. Vilenkin, Phys. Lett. **107B**, 47 (1981).
[10] S. Ölmez, V. Mandic, and X. Siemens, Phys. Rev. D **81**, 104028 (2010).
[11] S. A. Sanidas, R. A. Battye, and B. W. Stappers, Phys. Rev. D **85**, 122003 (2012).
[12] L. P. Grishchuk, Pis'ma Zh. Tekh. Fiz. **23**, 326 (1976).
[13] L. P. Grishchuk, Phys. Usp. **48**, 1235 (2005).
[14] P. A. Rosado and A. Sesana, Mon. Not. R. Astron. Soc. **439**, 3986 (2014).
[15] P. A. Rosado, A. Sesana, and J. Gair, Mon. Not. R. Astron. Soc. **451**, 2417 (2015).
[16] V. Ravi, J. S. B. Wyithe, G. Hobbs, R. M. Shannon, R. N. Manchester, D. R. B. Yardley, and M. J. Keith, Astrophys. J. **761**, 84 (2012).
[17] B. Kocsis and A. Sesana, Mon. Not. R. Astron. Soc. **411**, 1467 (2011).
[18] M. Milosavljević and D. Merritt, Astrophys. J. **596**, 860 (2003).
[19] G. Desvignes *et al.* (to be published).
[20] M. Kramer and D. J. Champion, Classical Quantum Gravity **30**, 224009 (2013).
[21] E. S. Phinney, arXiv:astro-ph/0108028.
[22] M. V. Sazhin, Sov. Astron. **22**, 36 (1978).
[23] S. Detweiler, Astrophys. J. **234**, 1100 (1979).
[24] F. B. Estabrook and H. D. Wahlquist, Gen. Relativ. Gravit. **6**, 439 (1975).
[25] W. L. Burke, Astrophys. J. **196**, 329 (1975).
[26] L. S. Finn, S. L. Larson, and J. D. Romano, Phys. Rev. D **79**, 062003 (2009).
[27] C. M. F. Mingarelli and T. Sidery, Phys. Rev. D **90**, 062011 (2014).
[28] C. M. F. Mingarelli, T. Sidery, I. Mandel, and A. Vecchio, Phys. Rev. D **88**, 062005 (2013).
[29] J. Gair, J. D. Romano, S. Taylor, and C. M. F. Mingarelli, Phys. Rev. D **90**, 082001 (2014).
[30] S. R. Taylor and J. R. Gair, Phys. Rev. D **88**, 084001 (2013).
[31] G. B. Hobbs, R. T. Edwards, and R. N. Manchester, Mon. Not. R. Astron. Soc. **369**, 655 (2006).
[32] R. T. Edwards, G. B. Hobbs, and R. N. Manchester, Mon. Not. R. Astron. Soc. **372**, 1549 (2006).
[33] L. Lentati, S. R. Taylor, C. M. F. Mingarelli, A. Sesana, S. A. Sanidas, A. Vecchio, R. N. Caballero, K. J. Lee, R. van Haasteren, S. Babak *et al.*, arXiv:1504.03692.
[34] R. van Haasteren and Y. Levin, Mon. Not. R. Astron. Soc. **428**, 1147 (2013).
[35] L. Lentati, P. Alexander, M. P. Hobson, S. Taylor, and S. T. Balan, Phys. Rev. D **87**, 104021 (2013).
[36] R. van Haasteren and M. Vallisneri, Phys. Rev. D **90**, 104012 (2014).
[37] R. van Haasteren and M. Vallisneri, Mon. Not. R. Astron. Soc. **446**, 1170 (2015).
[38] R. M. Shannon and J. M. Cordes, Astrophys. J. **725**, 1607 (2010).
[39] G. Hobbs, A. G. Lyne, and M. Kramer, Mon. Not. R. Astron. Soc. **402**, 1027 (2010).
[40] N. J. Cornish and A. Sesana, Classical Quantum Gravity **30**, 224005 (2013).
[41] S. Babak and A. Sesana, Phys. Rev. D **85**, 044034 (2012).
[42] R. W. Hellings and G. S. Downs, Astrophys. J. Lett. **265**, L39 (1983).
[43] A. Sesana and A. Vecchio, Phys. Rev. D **81**, 104008 (2010).
[44] S. Babak, P. Brem, A. Lassus, A. Petiteau, P. Rosado, A. Sesana, S. Taylor *et al.*, European Pulsar Timing Array Limits on Continuous Gravitational Waves from Individual Supermassive Black Hole Binaries (to be published).
[45] J. C. Pinheiro and D. M. Bates, Stat. Comput. **6**, 289 (1996).
[46] A. Dresden, Bull. Am. Math. Soc. **26**, 385 (1920).
[47] R. Penrose, Math. Proc. Cambridge Philos. Soc. **51**, 406 (1955).
[48] R. N. Manchester, Classical Quantum Gravity **30**, 224010 (2013).
[49] R. Nan, D. Li, C. Jin, Q. Wang, L. Zhu, W. Zhu, H. Zhang, Y. Yue, and L. Qian, Int. J. Mod. Phys. D **20**, 989 (2011).
[50] G. Hobbs, S. Dai, R. N. Manchester, R. M. Shannon, M. Kerr, K. J. Lee, and R. Xu, arXiv:1407.0435.
[51] R. S. Booth, W. J. G. de Blok, J. L. Jonas, and B. Fanaroff, arXiv:0910.2935.
[52] G. H. Janssen, G. Hobbs, M. McLaughlin, C. G. Bassa, A. T. Deller, M. Kramer, K. J. Lee, C. M. F. Mingarelli, P. A. Rosado, S. Sanidas *et al.*, *Proc. Sci.*, AASKA14 (2015) 037.